

Construction and Rigorous Analysis of Quantum-Like States

Ethan Dickey¹, Abhijeet Vyas¹, and Sabre Kais²

¹Department of Computer Science, Purdue University, West Lafayette, IN 47907, USA

²Department of Electrical and Computer Engineering and Department of Chemistry, North Carolina State University, Raleigh, NC 27606

July 30, 2025

Abstract

Extending upon the observations of the emergence of quantum-like states from classical complex synchronized networks, this work adds mathematical rigor to the analysis of single Quantum-Like (QL) bits constructed by eigenvectors of the adjacency matrices of such networks. First, we rigorously show that symmetric construction of such networks (regular undirected/symmetric bipartite graph G_C connecting two regular undirected subgraphs G_A, G_B) leads to an equal superposition of the $|+\rangle, |-\rangle$ Hadamard states (with basis $|0\rangle, |1\rangle$ set from eigenvectors of the subgraphs), and provide an analysis of sufficient conditions on the network for construction of such states. Second, we prove two methods to construct any arbitrary single qubit state $|\psi\rangle = a|0\rangle + b|1\rangle$, $|a|^2 + |b|^2 = 1$ and provide a switching lemma for the boundaries of both methods. The first method of construction is by detuning the regularities of the two subgraphs and the second is by asymmetrically constructing the bipartite connection matrix C by allowing it to be directed, and then detuning those regularities. While the intuition is derived from the motivation of using complex synchronized networks for quantum information storage and computations, the proofs for constructing eigenvectors that interact in a quantum-like fashion only require the structure of the graph embedded in the adjacency matrix. Practically, this means that synchronization is not important to creating quantum-like bits, only that the edge weights are generally unit or close to unit and that the subgraphs are regular. As such, the results on combinations of random k -regular graphs (precisely Erdős-Rényi graphs) may be independently interesting.

1 Introduction

Synchronized networks occur in a wide variety of classical systems ranging from schools of fish, interacting bacterial networks, and blinking fireflies to power grid fluctuations and mechanisms underpinning memory processes in the brain [7, 18, 36, 37]. A particularly striking everyday example of a complex synchronized network is pedestrians crossing a footbridge. When the bridge is full or swaying, the complex network of pedestrians nonlinearly synchronizes into lockstep, leading to nontrivial oscillations in the bridge [12].

Synchronized networks – particularly those with dense or nearly regular connectivity – remain stable under surprisingly large perturbations (e.g., random removal of up to half of the edges, provided the network remains connected and the coupling strength exceeds the master stability condition¹ [8, 29]). Furthermore, their adjacency (or Laplacian) spectrum regularly exhibit a large spectral gap: one or more eigenvalues distinguishably separated from the rest of the spectrum. With such a robust spectral gap, one can ponder if stable computation can be done with such emergent eigenvalues and associated eigenvectors. Indeed, if such stability gives rise to emergent behaviors when these networks interact, it can allow insight into mechanisms underpinning such processes. A particularly relevant example of this is helping understand mechanisms in the human brain, and whether those complex synchronized networks are performing some kind of computation viewable from emergent eigenvectors of their structure.

Recently, Scholes has discovered that such networks can give rise to *quantum-like* behavior, in particular that interacting multiple carefully constructed complex synchronized networks gives rise to emergent coherent quantum states [31, 32]. By coupling multiple synchronized subnetworks in a medium-connectivity regime, the eigenvectors associated with emergent eigenvalues of the subgraphs interact in a way analogous to quantum coherence and interference.

Underpinning this behavior is the approximate regularity of the underlying graphs. For instance, in a random k -regular graph one has a unique top eigenvalue $\lambda_1 = k$, while the second eigenvalue satisfies $\lambda_2 \leq 2\sqrt{k-1} + o(1)$ with high probability by the Alon–Boppana and Friedman theorems [3, 19, 28] (specifically that a random regular

¹In essence, this means the coupling is strong enough, given the network's structure, that any small deviations between nodes die out, keeping the system synchronized. See also the overview in [1].

graph is “almost Ramanujan” with high probability), yielding a nonzero spectral gap $k - \lambda_2$ that protects the coherent mode from the spectral bulk.

Beyond idealized regular graphs, many natural and engineered networks are better modeled as Erdős-Rényi random graphs $G(n, p)$, with n labeled vertices and each of the $\binom{n}{2}$ possible edges present independently with probability p [13, 16], otherwise known as a Bernoulli random graph [15, 23]. In this model the degree of each node concentrates sharply around its mean np (by Chernoff bounds), and for

$$p \geq \frac{\log n + \omega(1)}{n}$$

the graph is connected with high probability. Spectrally, the adjacency matrix of $G(n, p)$ has a top eigenvalue

$$\lambda_1 = np + o(n),$$

almost surely (with probability tending to 1 as n tends to ∞), as originally proven by Juhasz (1978) [26]². This follows the work in [34], while the bulk of the spectrum lies in the interval

$$\lambda_{i \neq 1} \in \left[-2\sqrt{np(1-p)}, 2\sqrt{np(1-p)} \right] + o(\sqrt{n})$$

almost surely by the semicircle law for dense graphs [20]³, so that a gap

$$\lambda_1 - \lambda_2 \geq np - 2\sqrt{np(1-p)} \tag{1}$$

opens up whenever $np \gg \sqrt{np}$ (as $o(n) - o(\sqrt{n}) > 0$, if we abuse notation for intuition). Thus, even though Erdős-Rényi graphs are not exactly regular, they inherit a large spectral gap in the dense regime [14]. See Appendix A for further analysis of this particular spectral gap.

Refer to [34] for more background on the analysis of emergent eigenvalues of Erdős-Rényi graphs (Bernoulli random matrices). For further discussion of the bounds of the spectrum, especially when $np \gg n^{2/3}$, see [4, 17, 24]. Also relevant are Weyl’s Inequalities (or Weyl’s interlacing properties) [11, 22].

In summary, we can model many “real-life” networks as Erdős-Rényi (Bernoulli) random graphs and get similar results for the value of the top eigenvalue λ_1 and the robustness of the spectral gap $\lambda_1 - \lambda_2$ as with random k -regular graphs. Moving forward, this paper primarily considers random k -regular graphs with the goal of using the top eigenvalue’s eigenvector to perform robust (due to the spectral gap) quantum-like operations using graph manipulations.

Returning to synchronized networks, this spectral separation underpins both robustness and coherence. In the master-stability framework [8, 29], the stability of the synchronous manifold depends on the ratio of the largest to second-smallest eigenvalues of the coupling Laplacian. A large gap guarantees that only the principal mode (associated with uniform synchronization) persists, while all orthogonal perturbations decay. It is precisely this mechanism that both protects against massive connection loss in dense random topologies and allows coupled synchronized subnetworks to exhibit emergent, quantum-like coherent modes when arranged as in Scholes et al.’s construction [31, 32]. See also [7, 21, 37, 38].

More recently, similar studies showed that the product space of these regular graphs that model complex synchronized networks can robustly model a Hilbert space in a 1-1 mapping from the product basis of quantum states to the eigenstates of these graphs [35]. They go on to show how to encode quantum information in the steady state of a classical network [5], how to perform maps on the product space of these graphs that correspond to quantum gates and measurement [6], and that, under certain conditions, the state space of classical synchronized networks evolve according to unitary dynamics [33].

Separating slightly from the physical motivation derived from complex synchronized networks, this work studies the graphs required to give rise to such Quantum-Like (QL) behavior from a computer science and mathematical perspective. While the work in [35] provides a robust 1-1 mapping to the product basis of quantum states, explicit construction and manipulation of such states requires either taking the Cartesian product of two graphs or performing a unitary transformation on the state space of a QL-bit, which are both highly unintuitive and expensive operations, with the Cartesian product resulting in an exponentially larger graph. We demonstrate how to explicitly construct an arbitrary QL-bit for any $|\psi\rangle = a|0\rangle + b|1\rangle$, for $|a|^2 + |b|^2 = 1$, by manipulating well-understood graph properties and prove rigorously the existence of such states.

²Proposition 2 gives $\lim_{n \rightarrow \infty} \frac{\lambda_1}{n} = p \implies \lambda_1 = pn + o(n)$ for square symmetric matrices with $a_{ii} = 0$ and $a_{ij} =$ Bernoulli random variables with probability p . For a k -regular graph ($k < n$) with random edge deletions of probability $1 - p$ (giving average degree $d = kp$; this can be equivalently understood as “masking” the Bernoulli random graph with a k -regular 1s matrix), following the proof of Proposition 2, we modify the proof to say that for a given row i , the probability $\Pr\left(\left|\frac{1}{k} \sum_{j=1}^n a_{ij} - p\right| > \delta\right)$ is exponentially small, yielding $\lim_{k \rightarrow \infty} \frac{\lambda_1}{k} = p$ w.h.p. $\implies \lambda_1 = kp + o(n)$. This corrects a bug in the adaptation (of techniques in [23]) of the Bernoulli random matrix decomposition in [34] to directly provide that $\lambda_1^B = np$ is the largest eigenvalue for Bernoulli random graphs and that k -regular graphs with random edge deletions have $\lambda_1 = kp$ w.h.p. This holds in expectation for ensembles of Bernoulli random graphs trivially.

³In [20], using Theorem 1, eqn. (6), take $\sigma = \sqrt{p(1-p)}$ for Bernoulli random variables a_{ij} , and $O(n^{1/3} \log n) \in o(\sqrt{n})$ as $n \rightarrow \infty$, see also [40] for improved bounds.

2 Definitions

Let G be a graph represented by its adjacency matrix. In our construction, a single QL-bit is built from two subgraphs G_A and G_B with adjacency matrices A and B , respectively, as in Figure 1. Assume that:

- G_A is k_A -regular on n vertices, and G_B is k_B -regular on m vertices.
- Their Perron–Frobenius eigenvectors [30] are given by

$$V_A = \frac{1}{\sqrt{n}} \mathbf{1}_n, \quad V_B = \frac{1}{\sqrt{m}} \mathbf{1}_m, \quad (2)$$

with associated eigenvalues

$$\lambda_A = k_A, \quad \lambda_B = k_B. \quad (3)$$

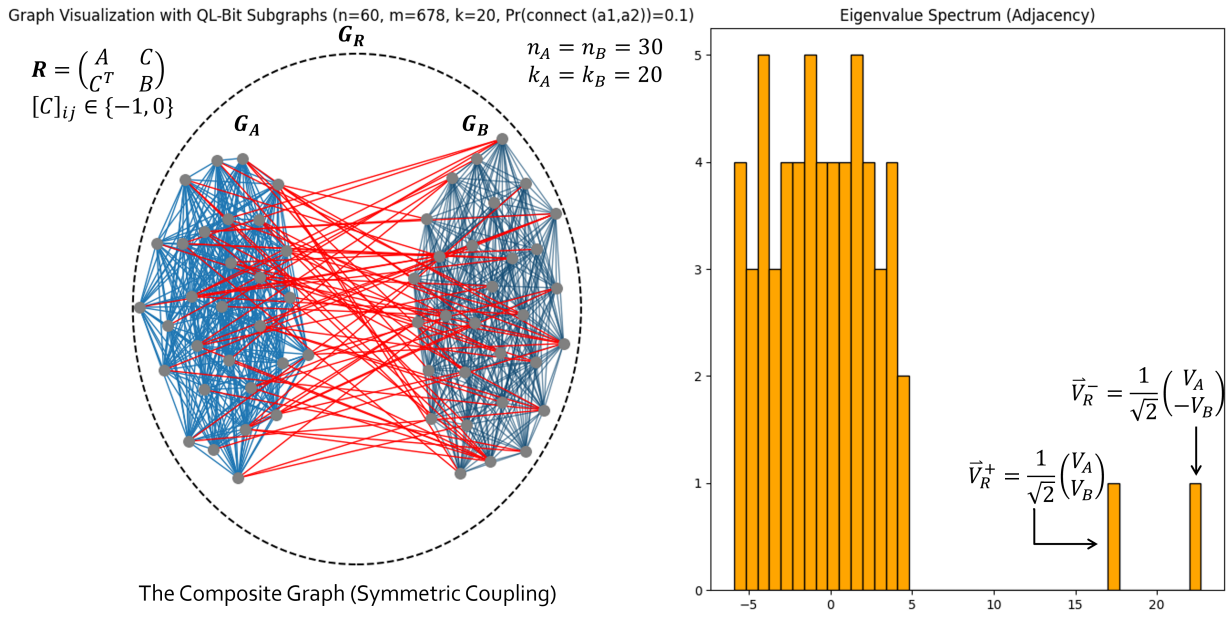


Figure 1: Regular graph and adjacency spectrum. Each subgraph has $n/2$ nodes. m -subgraph is set to None, indicating no edges deleted for a total of 678 edges $\approx 2 * (\# \text{edges in a } k\text{-regular subgraph of size } \frac{n}{2}) + \text{Pr}(\text{connect}) * (\# \text{possible (undirected) connecting edges}) = 2 * (k(\frac{n}{2})/2) + 0.1 * (\frac{n}{2})^2 = 20 * 30 + 0.1 * 30^2 = 690$. Note that the two emergent eigenvectors are approximately $20 \pm 3 = k \pm l$ for k -regular subgraphs G_A , G_B and approximately l -regular connecting graph G_C (randomly adding edges uniformly adds approximately $l := \frac{\# \text{edges added}}{v} * 2$ edges to each node). See Lemma 3.1 for more details.

In the simplest (symmetric) construction, the two subgraphs are coupled by a bipartite connection matrix C (of size $n \times m$, for n rows) with entries in $\{-1, 0\}$ (see footnote⁴), so that the composite adjacency matrix is⁵

$$R = \begin{pmatrix} A & C \\ C^T & B \end{pmatrix}.$$

When C is chosen to be l -regular (i.e. every vertex in the appropriate partition has exactly l connections with weight -1), one may define the *quantum-like* basis vectors as

$$\psi_+ \equiv |+\rangle = \frac{1}{\sqrt{2}} \left(\begin{pmatrix} V_A \\ \mathbf{0}_m \end{pmatrix} + \begin{pmatrix} \mathbf{0}_n \\ V_B \end{pmatrix} \right) = \frac{1}{\sqrt{2}} \begin{pmatrix} V_A \\ V_B \end{pmatrix}, \quad \psi_- \equiv |-\rangle = \frac{1}{\sqrt{2}} \begin{pmatrix} V_A \\ -V_B \end{pmatrix}. \quad (4)$$

We note here that the choice of the $|\pm\rangle$ basis (the Hadamard basis) allows for simplified analysis considering emergent eigenvectors, but one could have equivalently chosen the computational basis over $|0\rangle$, $|1\rangle$, defined as implied in the equation for ψ_+ .

⁴Due to motivation from complex synchronized networks, connecting edges are usually negative, $[C]_{ij} \in \{-1, 0\}$. In the theoretical analysis, having negative connection edges $[C]_{ij} \in \{-1, 0\}$ only switches the top two (emergent) eigenvalues, putting the eigenvalue corresponding to $|-\rangle$ above the one corresponding to $|+\rangle$. This is why the basis is chosen as $|\mp\rangle$ as opposed to the standard Hadamard basis $|\pm\rangle$.

⁵ R is precisely the adjacency matrix of a signed graph, where each nonzero entry carries a ± 1 sign. For a comprehensive survey of the adjacency spectra of signed graphs (including basic eigenvalue bounds, interlacing, and connections to two-graphs), see [10].

The goal is to construct an emergent eigenvector of R corresponding to an arbitrary state

$$\psi = a\psi_+ + b\psi_-, \quad \text{with} \quad |a|^2 + |b|^2 = 1.$$

In our treatment, we shall consider two methods for tuning the state:

1. Varying the regularities k_A and k_B (“detuning”) in the symmetric coupling, and
2. Allowing the off-diagonal coupling (C) to be directed (asymmetric) so that the two coupling blocks differ.

We also consider allowing edge weights continuously in $[-1, 1]$ rather than in $\{\pm 1, 0\}$ in Section 6, although this turns out to be not well physically motivated and trivially all-powerful.

3 Symmetric Construction and Detuning

The value of the top eigenvalues of R were previously only noted as observations in [6]. Here, we rigorously prove their existence and thereby show their exact construction.

Lemma 3.1 (Composition of Eigenvectors of R). *Let G_R be constructed from two disjoint k -regular subgraphs G_A and G_B , each of order n , with entries $[A]_{ij}, [B]_{ij} \in \{0, 1\}$, coupled by an l -regular bipartite graph G_C with undirected connection matrix C (with $[C]_{ij} \in \{-1, 0\}$). If V_A and V_B are the normalized eigenvectors corresponding to the largest eigenvalues of A and B , respectively, as in Equation (2), then the vectors*

$$V_R^- = \frac{1}{\sqrt{2}} \begin{pmatrix} V_A \\ -V_B \end{pmatrix} = |-\rangle \quad \text{and} \quad V_R^+ = \frac{1}{\sqrt{2}} \begin{pmatrix} V_A \\ V_B \end{pmatrix} = |+\rangle$$

are eigenvectors of

$$R = \begin{pmatrix} A & C \\ C^T & B \end{pmatrix}$$

with eigenvalues

$$\lambda_- = k + l \quad \text{and} \quad \lambda_+ = k - l, \tag{5}$$

respectively.

Proof. Since G_A and G_B are k -regular, by the Perron-Frobenius theorem,

$$AV_A = kV_A, \quad BV_B = kV_B,$$

and with $n = m$,

$$V_A = V_B = \frac{1}{\sqrt{n}} \mathbf{1}_n.$$

Furthermore, by the l -regularity and choice of signs in C , one has

$$CV_B = -lV_A \quad \text{and} \quad C^T V_A = -lV_B. \tag{6}$$

For

$$V_R^- = \frac{1}{\sqrt{2}} \begin{pmatrix} V_A \\ -V_B \end{pmatrix},$$

we compute:

$$RV_R^- = \frac{1}{\sqrt{2}} \begin{pmatrix} AV_A - CV_B \\ C^T V_A - BV_B \end{pmatrix} = \frac{1}{\sqrt{2}} \begin{pmatrix} kV_A + lV_A \\ -lV_B - kV_B \end{pmatrix} = (k + l)V_R^-. \tag{7}$$

A similar calculation shows that

$$RV_R^+ = (k - l)V_R^+.$$

□

The authors note that while the physical motivation from complex synchronized networks supports the use of $[C]_{ij} \in \{-1, 0\}$, modifying Lemma 3.1 to use $[C]_{ij} \in \{0, 1\}$ only changes the associated eigenvalues (switching the two emergent eigenvalues) of V_R^- and V_R^+ from Equation (5) to

$$\lambda_- = k - l \quad \text{and} \quad \lambda_+ = k + l.$$

Furthermore, by requiring V_R^- and V_R^+ to be eigenvectors of R , we have the following corollary.

Corollary 3.2 (Order of Subgraphs of R). *Let G_R be constructed from two disjoint k -regular subgraphs G_A and G_B , with orders n, m and entries $[A]_{ij}, [B]_{ij} \in \{0, 1\}$, coupled by a bipartite graph G_C with undirected connection matrix C (with $[C]_{ij} \in \{-1, 0\}$).*

We have that V_R^- and V_R^+ are normalized eigenvectors of R , as defined in Lemma 3.1, with dimensionality $n + m$ and eigenvalues λ_- and λ_+ , if and only if

- (a) $n = m$,
- (b) C and C^T are l -regular for some l (each row and column of C sums to l),
- (c) $\lambda_- = k + l$ and $\lambda_+ = k - l$ (for eigenvectors V_R^- and V_R^+), and
- (d) R is $(k + l)$ -regular.

In particular, item (b) is the necessary and sufficient condition and items (c) and (d) are sufficient. Furthermore, (d) \iff (c) by Perron-Frobenius, (d) \iff (b) by k -regularity of A and B , and (b) \implies C is square ($nl = ml$) \implies (a).

Proof. It suffices to show that V_R^- and V_R^+ are eigenvectors of $R \iff$ item (b).

(\implies) For

$$V_R^+ = \frac{1}{\sqrt{2}} \begin{pmatrix} V_A \\ V_B \end{pmatrix},$$

we compute:

$$R V_R^+ = \frac{1}{\sqrt{2}} \begin{pmatrix} A V_A + C V_B \\ C^T V_A + B V_B \end{pmatrix} = \frac{1}{\sqrt{2}} \begin{pmatrix} k V_A + C V_B \\ C V_A + k V_B \end{pmatrix}.$$

By the definition of eigenvectors,

$$\frac{1}{\sqrt{2}} \begin{pmatrix} k V_A + C V_B \\ C V_A + k V_B \end{pmatrix} = \lambda_R \begin{pmatrix} V_A \\ V_B \end{pmatrix},$$

which yields equations

$$\begin{aligned} k V_A + C V_B &= \lambda_R V_A \quad \text{and} \quad C^T V_A + k V_B = \lambda_R V_B \\ \implies C V_B &= (\lambda_R - k) V_A \quad \text{and} \quad C^T V_A = (\lambda_R - k) V_B. \end{aligned} \tag{8}$$

As $V_A = \mathbf{1}_n$ and $V_B = \mathbf{1}_m$, $C V_B$ and $C^T V_A$ must produce constants times all ones vectors, forcing all row sums to be equal and all column sums to be equal:

$$\sum_i [C]_{ij} = l_A \quad \forall j \quad \text{and} \quad \sum_j [C]_{ij} = l_B \quad \forall i$$

Making Equation (8) into

$$\begin{aligned} l_A V_A &= (\lambda_R - k) V_A \quad \text{and} \quad l_B V_B = (\lambda_R - k) V_B \\ \implies l_A + k &= \lambda_R \quad \text{and} \quad l_B + k = \lambda_R \\ \implies l_A &= l_B \end{aligned}$$

Thus, C and C^T are l -regular.

(\iff) This follows from (b) \iff (d) and either the Perron-Frobenius theorem or (a) and Lemma 3.1. □

3.1 Arbitrary QL-Bit State

Now, to construct an arbitrary QL-bit state, we allow the regularities of A and B to differ. Define tunable parameter

$$\Delta := \frac{k_A - k_B}{2l} \tag{9}$$

as the average of the two subgraph eigenvalues divided by the regularity of the bipartite connection matrix C .

Theorem 3.3 (Arbitrary Quantum-Like State Construction). *Let G_R be constructed from two disjoint regular subgraphs G_A and G_B , with regularities k_A, k_B , each of order n , with entries $[A]_{ij}, [B]_{ij} \in \{0, 1\}$, coupled by an l -regular bipartite graph G_C with undirected connection matrix C (with $[C]_{ij} \in \{-1, 0\}$). Let V_A, V_B be the normalized eigenvectors corresponding to the largest eigenvalues λ_A, λ_B of A, B , respectively, as in Equations (2) and (3), and basis vectors $|+\rangle, |-\rangle$ be defined as in Equation (4). Let the vector*

$$\begin{aligned} |\psi\rangle &:= V_R = a|+\rangle + b|-\rangle = \begin{pmatrix} \omega_1 V_A \\ \omega_2 V_B \end{pmatrix} \quad \text{with} \\ \omega_1 &:= \frac{1}{\sqrt{2}}(a+b), \quad \omega_2 := \frac{1}{\sqrt{2}}(a-b), \quad \text{s.t.} \\ |a|^2 + |b|^2 &\equiv |\omega_1|^2 + |\omega_2|^2 = 1 \end{aligned} \quad (10)$$

define an arbitrary quantum-like state. For $|a| \neq |b|$, if the regularities k_A, k_B , and l are tuned proportionally by the condition

$$\Delta = \frac{2ab}{b^2 - a^2} = \frac{\omega_2^2 - \omega_1^2}{2\omega_1\omega_2}, \quad (11)$$

then $|\psi\rangle$ is an eigenvector of

$$R = \begin{pmatrix} A & C \\ C^T & B \end{pmatrix}$$

with eigenvalue

$$\lambda_R = k_A - \frac{\omega_2}{\omega_1}l \stackrel{(9,11)}{=} k_B - \frac{\omega_1}{\omega_2}l. \quad (12)$$

(Notation $\stackrel{(9,11)}{=}$ indicates that step was taken using Equations (9) and (11).)

Proof. It suffices to show that $|\psi\rangle$ is an eigenvector of R with eigenvalue λ_R given Equation (11).

Solving Equations (9) and (11) for k_A and k_B yields

$$k_A = k_B + \frac{\omega_2^2 - \omega_1^2}{\omega_1\omega_2}l, \quad k_B = k_A - \frac{\omega_2^2 - \omega_1^2}{\omega_1\omega_2}l. \quad (13)$$

We proceed with solving the eigenvalue equation.

$$R|\psi\rangle = \begin{pmatrix} A & C \\ C^T & B \end{pmatrix} \begin{pmatrix} \omega_1 V_A \\ \omega_2 V_B \end{pmatrix} \quad (14)$$

$$= \begin{pmatrix} \omega_1 A V_A + \omega_2 C V_B \\ \omega_1 C^T V_A + \omega_2 B V_B \end{pmatrix} \quad (15)$$

$$\stackrel{(3,6)}{=} \begin{pmatrix} \omega_1 k_A V_A - \omega_2 l V_A \\ -\omega_1 l V_B + \omega_2 k_B V_B \end{pmatrix} \quad (16)$$

$$\stackrel{(13)}{=} \begin{pmatrix} \left(\omega_1 \frac{\omega_2^2 - \omega_1^2}{\omega_1\omega_2} l + \omega_1 k_B - \omega_2 l \right) V_A \\ \left(-\omega_2 \frac{\omega_2^2 - \omega_1^2}{\omega_1\omega_2} l + \omega_2 k_A - \omega_1 l \right) V_B \end{pmatrix} \quad (17)$$

$$= \begin{pmatrix} \left(-\frac{\omega_1^2}{\omega_2} l + \omega_1 k_B \right) V_A \\ \left(\frac{\omega_2^2}{\omega_1} l + \omega_2 k_A \right) V_B \end{pmatrix} \quad (18)$$

$$\stackrel{(12)}{=} \begin{pmatrix} \omega_1 \lambda_R V_A \\ \omega_2 \lambda_R V_B \end{pmatrix} = \lambda_R \begin{pmatrix} \omega_1 V_A \\ \omega_2 V_B \end{pmatrix} \quad (19)$$

(Once more for cross-field notation clarity: $\stackrel{(3,6)}{=}$ indicates that step was taken using Equations (3) and (6).) \square

In the same notion as after Lemma 3.1, using $[C]_{ij} \in \{0, +1\}$ only changes Equation (12) to

$$\lambda_R = k_A + \frac{\omega_2}{\omega_1}l = k_B + \frac{\omega_1}{\omega_2}l. \quad (20)$$

The math in Theorem 3.3 remains the same except that l flips signs in every equation, including in the definition of Δ (Equation (9)).

Thus, any state of the form $a\psi_+ + b\psi_-$ (with $a^2 + b^2 = 1$) may be realized via appropriate choices of k_A , k_B , and l (i.e. Δ), provided $|a| \neq |b|$. However, note that as $|a| \rightarrow |b| = \frac{1}{\sqrt{2}}$ we have

$$\lim_{|a| \rightarrow |b|} \Delta = \infty. \quad (21)$$

This divergence implies that a perfectly balanced state via detuning alone would require an unbounded difference in the subgraph regularities. This is further illustrated in Figure 2, where the set of possible $|\psi\rangle$ values (cylinder, defined by $|a|^2 + |b|^2 = 1$ for $a, b \in x\text{-axis, } y\text{-axis}$), plotted against tunable parameter $\Delta \equiv z\text{-axis}$, are constrained to the feasible regions (lines running vertically along the walls of the cylinder) of Equation (11). Indeed, as $|x| \rightarrow |y|$, the feasible regions grow to ∞ . A solution to this is found in the proof for the asymmetric coupling construction, Lemma 4.1 (by inverting its Δ_C), and applied to symmetric coupling in Section 4.2.

3.2 Constraints on Symmetric Coupling

We proceed with an explicit construction of Δ given a target qubit state $|\psi\rangle$.

Example 3.1 (Constructing a Skewed Superposition via Detuning). Given a target single-qubit state $|\psi\rangle$ determined by parameters $a = \sqrt{\frac{1}{3}}$, $b = \sqrt{\frac{2}{3}}$, we can construct a graph based on the following method:

1. Compute Δ as $\Delta = \frac{2ab}{b^2 - a^2} = \frac{2\sqrt{2/9}}{1/3} = 2\sqrt{2} \approx 2.8284$
2. Set the regularities of A , B , and C such that $2\sqrt{2} = \frac{k_A - k_B}{2l}$. For example, in a $n/2 = 30$ node graph (each subgraph having 30 nodes), if k_A and k_B are set prior, in order to get a more robust emergent state, as $k_A = 25$, $k_B = 20$, then $l = \frac{5\sqrt{2}}{8} \approx 0.8838835$.

One may notice that this example sets the regularity of the bipartite connection matrix C to a non-integer value. While mathematically this matters little if we allow $[C]_{ij} \in \mathbb{R}$ (or even $\in \mathbb{C}$), as discussed in Section 6, using the graph intuition, where regularity is defined by the number of edges coming out of a particular node, non-integer values do not make sense. This constraint is tightened further by restricting to simple graphs (no multiedges nor self-loops). In particular, for a graph G_R with $2n$ nodes (n nodes per subgraph G_A and G_B), one can impose the constraints

$$\begin{aligned} |k_A - k_B| &< n, \\ |l| &< n, \\ k_A, k_B, l &\neq 0, \quad \text{and} \\ k_A, k_B, l &\in \mathbb{Z}. \end{aligned} \quad (22)$$

Which, intuitively, say that the valency of any one node cannot be more than the number of nodes in the target subgraph (first and second conditions), that no graph can have a regularity of 0 (no edges; third condition), and that the regularities of all three graphs (including bipartite connection graph G_C) must be integers (last condition). Together, these give the exact bound

$$|\Delta| < n, \quad \Delta \in \mathbb{Q}$$

(for the group of rational numbers \mathbb{Q}) in the maximal setting of $k_A = k_B - 1$ and $l = 1$ (see Equation (9)). Furthermore, we can precisely relate the possible values of a and b in Equation (10) to Δ by the bounds

$$\begin{aligned} a &= \pm \frac{1}{\sqrt{2}} \sqrt{\left(1 \pm \frac{1}{\sqrt{\Delta^2 + 1}}\right)} \\ b &= \pm \frac{1}{\sqrt{2}} \sqrt{\left(1 \mp \frac{1}{\sqrt{\Delta^2 + 1}}\right)} \end{aligned} \quad (23)$$

given $a^2 + b^2 = 1 \implies b = \pm\sqrt{1 - a^2}$. This leads to 4 possible sign combinations indicating what values of a and b each formula is valid for,

$$\begin{aligned} a(+, +) &\implies +a, |a| > |b| \\ a(+, -) &\implies +a, |b| > |a| \\ a(-, -) &\implies -a, |a| > |b| \\ a(-, +) &\implies -a, |b| > |a| \end{aligned} \quad (24)$$

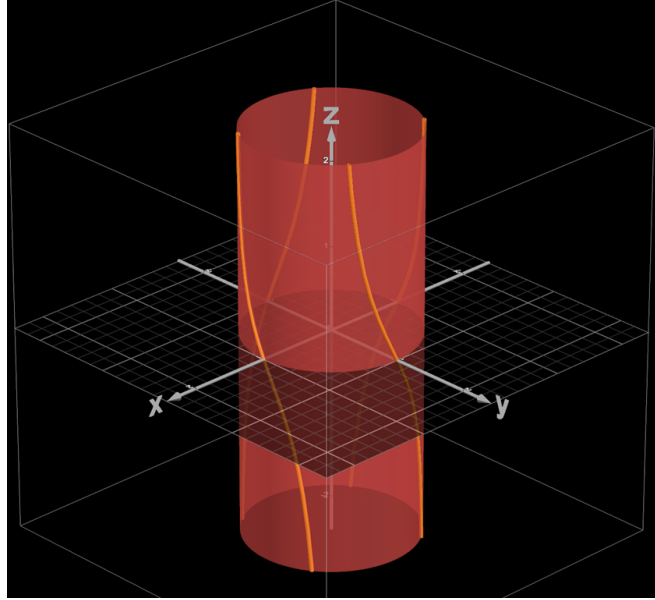


Figure 2: Basic visualization of the bounds of Δ applied to $|\psi\rangle$. The x-axis is a , the y-axis is b , and the z-axis is Δ . The cylinder is defined by the circle (extended to 3D) $a^2 + b^2 = 1$ and is the set of possible points under the definition of $|\psi\rangle$ in Equation (10). By plotting it against Δ , we can see what values $|\psi\rangle$ are possible given the equation for Δ , Equation (11), as shown by the four lines running up the cylinder. See text after Theorem 3.3 for more.

where $a(\cdot, \cdot)$ informally references a choice of signs in Equation (23). Perhaps more intuitively, these sign combinations define 4 quadrants (extended to 3 dimensions by Δ) of a vs b defined by boundaries that go to ∞ as $|a| \rightarrow |b|$.

These practical constraints on Δ are illustrated in Figure 3. The constraint $\Delta \in \mathbb{Q}$ is shown by the xy -planes at (demonstratively) integer values on the z -axis ($\equiv \Delta$). The four possible a combinations ($\pm \otimes \pm$) in Equation (23) are shown as vertical planes and intersect precisely with the feasible lines more easily seen in Figure 2 and discussed above. The possible values for $|\psi\rangle$ are therefore understood as the intersection of the xy -planes with the feasible lines. As n increases, the ability of Equation (9) to approximate $|\psi\rangle$ increases precisely as the growth of a denominator increases the ability of a fraction to approximate a real number (i.e. the rational numbers). We provide a list of equations to reconstruct the graph in Appendix B.

4 Asymmetric Coupling Construction

To avoid the divergence in Δ (when $|a| \rightarrow |b| \equiv \omega_1, \omega_2 \rightarrow 0$), we allow the coupling to be directed. Replace the single matrix C by two matrices C_A and C_B :

$$R = \begin{pmatrix} A & C_A \\ C_B & B \end{pmatrix},$$

with

$$C_A V_B = -l_A V_A, \quad C_B V_A = -l_B V_B. \quad (25)$$

By defining the tunable parameter

$$\Delta_C := \frac{l_A}{l_B}, \quad (26)$$

and sets $l_A = 0$, one obtains the emergent eigenvector

$$V_R = \begin{pmatrix} 0 \\ V_B \end{pmatrix} = \frac{1}{\sqrt{2}}(|+\rangle - |-\rangle) = |1\rangle,$$

one of the two states of issue in Equation (21) ($a \rightarrow -b = -\frac{1}{\sqrt{2}}, |1\rangle$). The other ($a \rightarrow b = \frac{1}{\sqrt{2}}, |0\rangle$) is created when $l_B = 0$. More generally, by tuning l_A and l_B independently one can realize any desired (near-balanced) state without forcing Δ_C to diverge.

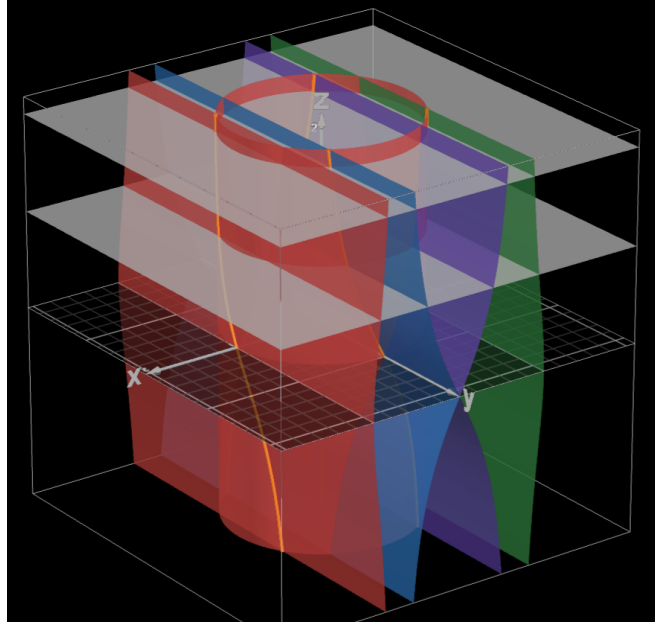


Figure 3: Full visualization of the bounds of Δ applied to $|\psi\rangle$. The x-axis is a , the y-axis is b , and the z-axis is Δ . Refer to Figure 2 for introduction. Added to this plot are six planes. The vertical four planes are defined by the four variations of a in Equation (23) ($\pm \otimes \pm$) and demonstrate the possible a values given tunable parameter Δ . As analyzed in Equation (22), Δ is also constrained to be a rational number. For simplicity, the plot shows only positive integer values of Δ as xy-planes perpendicular to the z-axis. Feasible values for $|\psi\rangle$ are therefore constrained to intersections of the xy-planes with the feasible vertical lines.

Definition 4.1 (Directed Regular Graph). An unweighted directed graph G_D is l -regular if the sum of the rows of its adjacency matrix D (the outgoing edges) are equal to l :

$$\sum_j [D]_{ij} = l \quad \forall i.$$

Lemma 4.1 (Balanced QL-Bit via Asymmetric Coupling). *Let G_R be constructed from two disjoint regular subgraphs G_A and G_B , with regularities k_A, k_B , each of order n , with entries $[A]_{ij}, [B]_{ij} \in \{0, 1\}$, coupled by bipartite graph G_C with l_A, l_B -regular directed connection matrices C_A, C_B (with $[C_A]_{ij}, [C_B]_{ij} \in \{-1, 0\}$). Let V_A, V_B be the normalized eigenvectors corresponding to the largest eigenvalues λ_A, λ_B of A, B , respectively, as in Equations (2) and (3), and basis vectors $|+\rangle, |-\rangle$ be defined as in Equation (4). Let the vector $|\psi\rangle$ be an arbitrary quantum-like state with parameters a, b, ω_1, ω_2 be defined as in Equation (10). If the regularities of the subgraphs are equal, $k_A = k_B$, and l_A, l_B are tuned proportionally by the condition*

$$\Delta_C = \frac{a+b}{a-b} = \frac{\omega_1^2}{\omega_2^2} \quad (27)$$

then $|\psi\rangle$ is an eigenvector of

$$R = \begin{pmatrix} A & C_A \\ C_B & B \end{pmatrix}$$

with eigenvalue

$$\begin{aligned} \lambda_R &= k_A - \frac{\omega_2}{\omega_1} l_A \stackrel{(26,27)}{=} k_B - \frac{\omega_1}{\omega_2} l_B \\ &= k - \frac{\omega_2}{\omega_1} l_A \stackrel{(26,27)}{=} k - \frac{\omega_1}{\omega_2} l_B \end{aligned} \quad (28)$$

similarly to Theorem 3.3, Equation (12).

Proof. We note for completeness that by definition (Equation (10)), it cannot be the case that $\omega_1 = \omega_2 = 0$. Thus, if $\omega_1 \text{ XOR } \omega_2 = 0$, one may simply invert the definition and target equation for Δ_C to achieve the desired state, as the equations derived for Δ_C began as $\omega_1^2 l_B - \omega_2^2 l_A = 0$. Further details provided in Appendix C.

Otherwise, it suffices to show that $|\psi\rangle$ is an eigenvector of R with eigenvalue λ_R given Equation (27).

Solving Equations (26) and (27) for l_A and l_B yields

$$l_A = \frac{\omega_1^2}{\omega_2^2} l_B, \quad l_B = \frac{\omega_2^2}{\omega_1^2} l_A. \quad (29)$$

We proceed with solving the eigenvalue equation.

$$R|\psi\rangle = \begin{pmatrix} A & C_A \\ C_B & B \end{pmatrix} \begin{pmatrix} \omega_1 V_A \\ \omega_2 V_B \end{pmatrix} \quad (30)$$

$$= \begin{pmatrix} \omega_1 A V_A + \omega_2 C_A V_B \\ \omega_1 C_B V_A + \omega_2 B V_B \end{pmatrix} \quad (31)$$

$$\stackrel{(3.25)}{=} \begin{pmatrix} \omega_1 k V_A - \omega_2 l_A V_A \\ -\omega_1 l_B V_B + \omega_2 k V_B \end{pmatrix} \quad (32)$$

$$= \begin{pmatrix} \omega_1 \left(k - \frac{\omega_2}{\omega_1} l_A \right) V_A \\ \omega_2 \left(k - \frac{\omega_1}{\omega_2} l_B \right) V_B \end{pmatrix} \quad (33)$$

$$\stackrel{(28)}{=} \begin{pmatrix} \omega_1 \lambda_R V_A \\ \omega_2 \lambda_R V_B \end{pmatrix} = \lambda_R \begin{pmatrix} \omega_1 V_A \\ \omega_2 V_B \end{pmatrix} \quad (34)$$

□

Explicitly, the primary differences between Lemma 4.1 and Theorem 3.3 are the following:

1. The lemma allows $C_A \neq C_B^T$, i.e. the bipartite connection graph G_C to be directed, but still require that both be regular (see Definition 4.1) with entries $\in [-1, 0]$. This loosens the setting.
 - The interpretation of C_A is all of the outgoing edges from $A \rightarrow B$, and its (row) regularity is over the outgoing edges from A . Similarly for C_B .
2. The lemma tightens the setting by requiring $k_A = k_B$, the regularities of A and B to match. The connection between these two relaxations is made explicit in Appendix C.
3. The theorem requires $|a| \neq |b| \equiv (\omega_1 \text{ or } \omega_2) \neq 0$, but the lemma has no such constraint. If $(a = b \text{ or } a = -b) \equiv (\omega_1 \text{ or } \omega_2) = 0$, one may simply invert the definition and target equation for Δ_C to achieve the desired state. Both a and b cannot be simultaneously 0 by definition.

In the same notion as after lemma 3.1 and theorem 3.3, using $[C]_{ij} \in \{0, +1\}$ only changes Equation (28) to

$$\lambda_R = k + \frac{\omega_2}{\omega_1} l_A = k + \frac{\omega_1}{\omega_2} l_B. \quad (35)$$

The math in Lemma 4.1 remains the same except that l_A, l_B flip signs in every equation.

Thus, any state of the form $a\psi_+ + b\psi_-$ (with $a^2 + b^2 = 1$) may be realized via appropriate choices of l_A and l_B (i.e. Δ_C). If $l_A = 0$ or $l_B = 0$, it is trivial to define $\Delta_C = \Delta_C^{-1}$ and invert Equation (27). As discussed in the proof, by definition, it cannot be the case that $\omega_1 = \omega_2 = 0$.

This divergence implies that a perfectly balanced state via detuning alone would require an unbounded difference in the subgraph regularities. This is further illustrated in Figure 2, where the set of possible $|\psi\rangle$ values (cylinder, defined by $a, b \equiv x\text{-axis, } y\text{-axis}$) are constrained to the feasible regions (lines running vertically along the walls of the cylinder) of Equation (27). Indeed, as $|x| \rightarrow |y|$, the feasible regions grow to ∞ . We proceed with an explicit construction of Δ given a target qubit state $|\psi\rangle$.

Example 4.1 (Constructing a Skewed Superposition via Detuning). Given a target single-qubit state $|\psi\rangle$ determined by parameters $a = \sqrt{\frac{1}{3}}$, $b = \sqrt{\frac{2}{3}}$, we can construct a graph based on the following method:

1. Compute Δ_C as $\Delta_C = \frac{a+b}{a-b} = \frac{1+\sqrt{2}}{\sqrt{3}} \approx 1.3938$
2. Set the regularities of A, B , and C such that $\frac{1+\sqrt{2}}{\sqrt{3}} = \frac{l_A}{l_B}$. For example, in a $n/2 = 30$ node graph (each subgraph having 30 nodes), if we set a minimum threshold for the regularities l_A, l_B to 15 in order to get a more robust emergent state, then $10 * l_A = 10 * (1 + \sqrt{2}) \approx 24.1421$, $10 * l_B = 10 * \sqrt{3} \approx 17.3205$.

One may notice that this example sets the regularity of the bipartite connection matrix C to a non-integer value. While mathematically this matters little if we allow $[C]_{ij} \in \mathbb{R}$ (or even $\in \mathbb{C}$), as discussed in Section 6, using the graph intuition, where regularity is defined by the number of edges coming out of a particular node, non-integer values do not make sense. This constraint is tightened further by restricting to simple graphs (no multiedges nor self-loops). In particular, for a graph G_R with $2n$ nodes (n nodes per subgraph G_A and G_B), one can impose the constraints

$$\begin{aligned} |l_A - l_B| &< n, \\ l_A, l_B, k &\neq 0, \quad \text{and} \\ l_A, l_B, k &\in \mathbb{Z}. \end{aligned} \tag{36}$$

Which, intuitively, say that the valency of any one node cannot be more than the number of nodes in the target subgraph (first condition), that no graph can have a regularity of 0 (no edges; second condition), and that the regularities of all three graphs must to be integers (last condition). Together, these give the exact bound

$$|\Delta_C| < n, \quad \Delta_C \in \mathbb{Q}$$

(for the group of rational numbers \mathbb{Q}) in the maximal setting of $l_A = n - 1$ and $l_B = 1$ (see Equation (26)). Furthermore, we can precisely relate the possible values of a and b in Equation (10) to Δ_C and Δ_C^{-1} by the bounds

$$\begin{aligned} a &= \pm \frac{1}{\sqrt{2}} \frac{\Delta_C + 1}{\sqrt{\Delta_C^2 + 1}} \\ b &= \pm \frac{1}{\sqrt{2}} \frac{\Delta_C - 1}{\sqrt{\Delta_C^2 + 1}}, \end{aligned} \tag{37}$$

given $a^2 + b^2 = 1 \implies b = \pm\sqrt{1 - a^2}$. This leads to 2 possible sign combinations for both Δ_C and Δ_C^{-1} ,

$$\begin{aligned} \Delta_C : a(+) &\implies a > b \\ a(-) &\implies b > a \\ \Delta_C^{-1} : a(+) &\implies a > -b \\ a(-) &\implies -b > a \end{aligned} \tag{38}$$

where $a(\cdot)$ informally references a choice of signs in Equation (37).

These practical constraints on Δ_C (Δ_C^{-1}) are illustrated in Figure 5. The constraint $\Delta_C \in \mathbb{Q}$ is shown by the xy-planes at (demonstratively) integer values on the z-axis ($\equiv \Delta_C, \Delta_C^{-1}$). The two possible a combinations (\pm) in Equation (37) are shown as vertical planes and intersect precisely with the feasible lines more easily seen in Figure 4 and discussed above. The possible values for $|\psi\rangle$ are therefore understood as the intersection of the xy-planes with the feasible lines. As n increases, the ability of Equation (26) to approximate $|\psi\rangle$ increases precisely as the growth of a denominator increases the ability of a fraction to approximate a real number (i.e. the rational numbers). We provide a list of equations to reconstruct the graph in Appendix B.

4.1 Switching Between Asymmetric Constructions

With simple observation of Figures 4 and 5 and eq. (38), we provide the following simple switching condition on which of Δ_C or Δ_C^{-1} to choose:

$$\begin{cases} \Delta_C & \text{if } \text{sign}(a) = -\text{sign}(b) \\ \Delta_C^{-1} & \text{if } \text{sign}(a) = \text{sign}(b) \end{cases} \tag{39}$$

And $\Delta_C = \Delta_C^{-1}$ when $a = 0$ or $b = 0$.

4.2 Switching Between Symmetric Constructions

Similarly to asymmetric coupling, we can invert Δ in Equations (9) and (11) to completely cover the divergence in Equation (21). This leads to an altered relationship between Δ^{-1} and a, b (compare: Equation (23)) defined by

$$\begin{aligned} a &= \pm \frac{1}{\sqrt{2}} \sqrt{\left(1 \pm \frac{\Delta}{\sqrt{\Delta^2 + 1}}\right)} \\ b &= \pm \frac{1}{\sqrt{2}} \sqrt{\left(1 \mp \frac{\Delta}{\sqrt{\Delta^2 + 1}}\right)} \end{aligned} \tag{40}$$

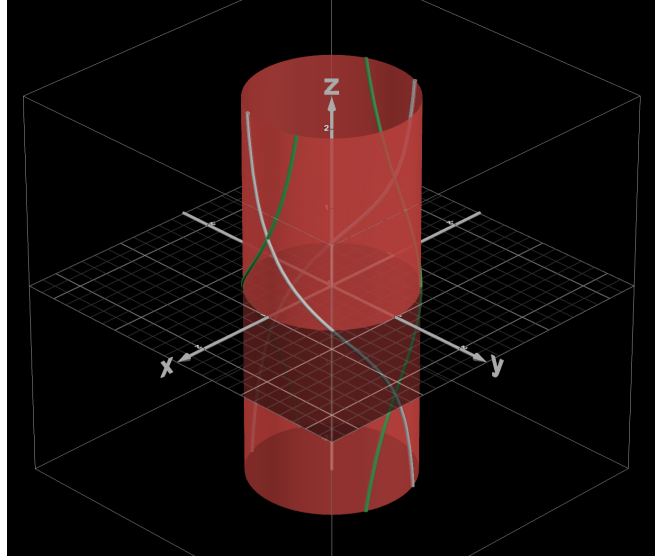


Figure 4: Basic visualization of the feasible values of Δ_C (green line, $\rightarrow \infty$ as $x \rightarrow y$) and Δ_C^{-1} (grey line, $\rightarrow \infty$ as $x \rightarrow -y$) applied to $|\psi\rangle$. The x-axis is a , the y-axis is b , and the z-axis is Δ_C (Δ_C^{-1}). The cylinder is defined by the circle (extended to 3D) $a^2 + b^2 = 1$ and is the set of possible points under the definition of $|\psi\rangle$ in Equation (10). By plotting it against Δ_C (Δ_C^{-1}), we can see what values $|\psi\rangle$ are possible given the equation for Δ_C (Δ_C^{-1}), Equation (27), as shown by the four lines running up the cylinder. See text after Lemma 4.1 for more.

and possible sign combinations (indicating what values of a and b each formula is valid for),

$$\begin{aligned} a(+, +) &\implies +a, -b \\ a(+, -) &\implies +a, +b \\ a(-, -) &\implies -a, +b \\ a(-, +) &\implies -a, -b \end{aligned} \tag{41}$$

where $a(\cdot, \cdot)$ informally references a choice of signs in Equation (40).

The feasible lines for Δ and Δ^{-1} can be seen together in Figure 6. Full visualization with Equation (40), as in Figure 3, is omitted for clarity but is available for reconstruction in Appendix B.

To determine when to switch between Δ and Δ^{-1} , we set $\Delta = \Delta^{-1}$ ($= \pm 1$) to get

$$a = \pm b(1 \pm \sqrt{2}).$$

Plugging in $a^2 + b^2 = 1$,

$$a = \pm \sqrt{\frac{2 \pm \sqrt{2}}{4}} \quad \text{and} \quad b = \pm \sqrt{\frac{2 \mp \sqrt{2}}{4}},$$

agreeing with the visible intersection points in Figure 6. We therefore provide the following switching condition on which of Δ or Δ^{-1} to choose:

$$\begin{cases} \Delta & \text{if } |a| \text{ or } |b| \leq \frac{1}{2}\sqrt{2 + \sqrt{2}} \\ \Delta^{-1} & \text{otherwise} \end{cases} \tag{42}$$

And $\Delta = \Delta^{-1}$ when $|a| =$ or $|b| = \frac{\sqrt{2 + \sqrt{2}}}{2}$.

5 Random Walk Interpretation

As an alternative to the quantum-state picture, we can view the composite graph G_R through the lens of classical random walks. Classically, the steady state (or stationary distribution) for a random walk on a graph is a vector containing the probability of being in each node if one ‘wanders’ from node to node uniformly randomly along edges. See [27] for background on random walks. By tracing how the structural parameters (k_A, k_B, l) fix both the target quantum-like state $|\psi\rangle = a|0\rangle + b|1\rangle$ and the walk’s stationary distribution, we see which degrees of freedom remain to optimize secondary criteria.

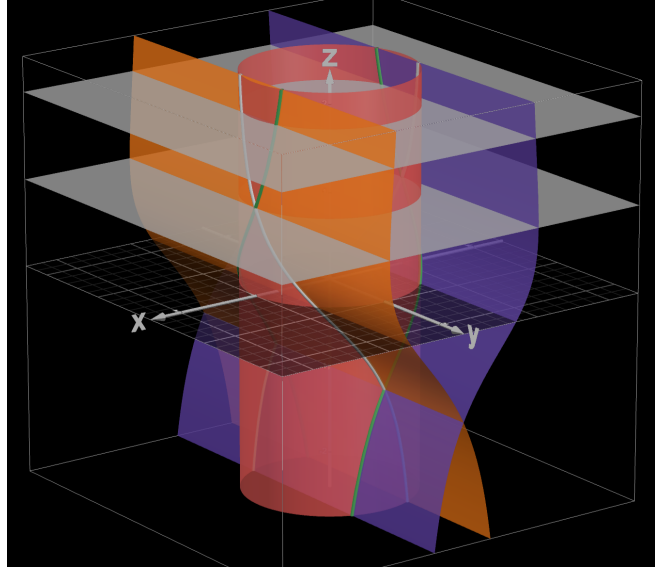


Figure 5: Full visualization of the feasible values of Δ_C (green line, $\rightarrow \infty$ as $x \rightarrow y$) and Δ_C^{-1} (grey line, $\rightarrow \infty$ as $x \rightarrow -y$) applied to $|\psi\rangle$. The x-axis is a , the y-axis is b , and the z-axis is Δ . Refer to Figure 4 for introduction. Added to this plot are four planes. The vertical two planes are defined by the two variations of a in Equation (37) (\pm) and demonstrate the possible a values given tunable parameter Δ_C (Δ_C^{-1}). As analyzed in Equation (36), Δ_C is also constrained to be a rational number. For simplicity, the plot shows only positive integer values of Δ_C as xy -planes perpendicular to the z -axis. Feasible values for $|\psi\rangle$ are therefore constrained to intersections of the xy -planes with the feasible vertical lines.

5.1 Fully Regular Graph

Let G_R be a (strongly) connected k -regular graph on $2n$ vertices, with adjacency matrix

$$R = \begin{pmatrix} A & C \\ C^T & B \end{pmatrix}, \quad \deg(i) = k \quad \forall i.$$

Define the simple random walk transition matrix

$$P = \frac{1}{k} R.$$

Since G_R is k -regular, P is doubly-stochastic (each row and column is a probability vector over next steps) and, by connectivity, irreducible. Thus, there is a unique stationary distribution, namely the uniform one. In the classical (probabilistic) picture we normalize in the L^1 -sense:

$$\pi = \left(\frac{1}{2n}, \frac{1}{2n}, \dots, \frac{1}{2n} \right), \quad \pi P = \pi, \quad \sum_i \pi_i = 1.$$

Equivalently, by Perron–Frobenius the principal **right**-eigenvector of P (the one for eigenvalue 1) may be chosen with unit Euclidean norm $\|v\|_2 = 1$,

$$v = \frac{1}{\sqrt{2n}} (1, 1, \dots, 1)^T.$$

Rewriting with respect to V_A and V_B in Equation (2), we get

$$v = \frac{1}{\sqrt{2}} \begin{pmatrix} V_A \\ V_B \end{pmatrix},$$

coinciding with the balanced quantum-like state $|+\rangle = \frac{1}{\sqrt{2}} (|0\rangle + |1\rangle)$ attained when $k_A = k_B$ and $l \neq 0$.

5.2 Undirected Detuning

When G_R is not regular but its two halves are k_A - and k_B -regular and connected by an l -regular bipartite matrix C , node degrees become

$$\deg(i) = \begin{cases} k_A + l, & i \in A, \\ k_B + l, & i \in B. \end{cases}$$

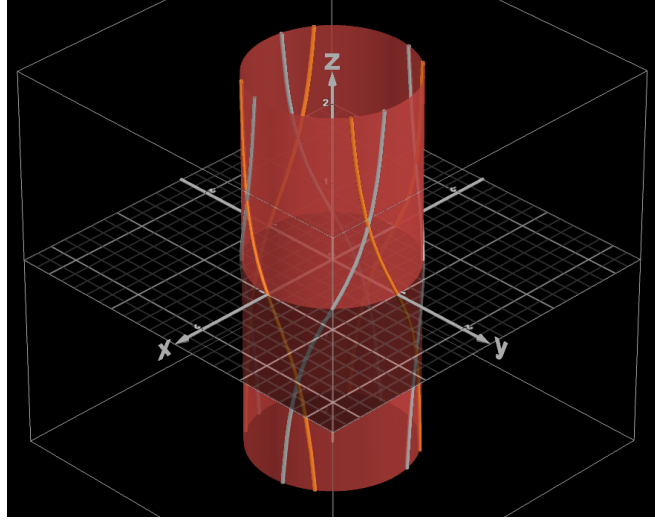


Figure 6: Symmetric Coupling: Basic visualization of the feasible values of Δ (orange line, $\rightarrow \infty$ as $|x| \rightarrow |y|$) and Δ^{-1} (grey line, $\rightarrow \infty$ as $x, y \rightarrow 0$) applied to $|\psi\rangle$. The x-axis is a , the y-axis is b , and the z-axis is $\Delta (\Delta^{-1})$. The cylinder is defined by the circle (extended to 3D) $a^2 + b^2 = 1$ and is the set of possible points under the definition of $|\psi\rangle$ in Equation (10). By plotting it against $\Delta (\Delta^{-1})$, we can see what values $|\psi\rangle$ are possible given the equation for $\Delta (\Delta^{-1})$, Equation (11), as shown by the eight lines running up the cylinder. See Section 4.2 for more.

Thus, the stationary distribution of the walk (defined as the top eigenvector of the transition matrix $P := D^{-1}R$, for diagonal degree matrix D) is

$$\pi_i = \frac{\deg(i)}{\sum_j \deg(j)} = \begin{cases} \frac{k_A + l}{n(k_A + k_B + 2l)}, & i \in A, \\ \frac{k_B + l}{n(k_A + k_B + 2l)}, & i \in B. \end{cases} \quad (43)$$

Introducing $X := k_A/l$, $Y := k_B/l$, and the detuning parameter $\Delta = (k_A - k_B)/(2l)$ (undirected version, from Equation (9)), we obtain

$$\pi_i = \begin{cases} \frac{X + 1}{2n(X + 1 - \Delta)}, & i \in A, \\ \frac{Y + 1}{2n(Y + 1 + \Delta)}, & i \in B. \end{cases} \quad (44)$$

By contrast, the quantum amplitudes (a, b) depend *only* on Δ (see Theorem 3.3 and eq. (11)), leaving the global scale X (and hence Y) free to tune other metrics—e.g., the spectral gap—without altering $|\psi\rangle$.⁶

5.3 Directed coupling

If the bipartite connector is directed with degrees (l_A, l_B) and we set $k_A = k_B$, as in Section 4, the same logic gives

$$\pi_i = \begin{cases} \frac{k + l_A}{n(2k + l_A + l_B)}, & i \in A, \\ \frac{k + l_B}{n(2k + l_A + l_B)}, & i \in B, \end{cases} \quad (45)$$

where again fixing the quantum amplitudes (a, b) pins down only the ratio $\Delta_C = l_A/l_B$ (see Lemma 4.1 and eq. (27)), leaving the global scales $X := l_A/k$ and $Y := l_B/k$ free.

5.4 Summary and Outlook

Matching a target quantum-like state $|\psi\rangle$ fixes certain *relative* degree ratios (e.g., Δ or Δ_C) while leaving a continuous manifold of absolute scalings (X, Y) at one's disposal. The classical stationary distribution is sensitive to those scalings and therefore encodes extra information beyond $|\psi\rangle$ —information that can be leveraged to optimize spectral separation, robustness, or hardware implementability in multi-bit extensions (see Section 7.1).

⁶For example, given $\Delta = 0.5$, there are a countably infinite number of ratios $X = \frac{k_A}{l}$ that satisfy $0.5 = \frac{k_A - k_B}{2l} \implies l = k_A - k_B$, such as $n = 40$, $X = 10$ (or 20) $\implies \pi_i = 0.0131$ (or 0.0128).

6 Real-Valued Bipartite Connection Matrix C

Allowing real edge weights, in short, makes construction of an arbitrary QL-bit state trivial. Furthermore, guided by the underlying motivation of in- and out-of-phase oscillators in complex synchronized networks, we find that real edge weights lack physical motivation. Generally, two oscillators are in-sync or out-of-sync, with anything in between being ill-defined and unstable.

We demonstrate the triviality by allowing a minimal relaxation, $[C]_{ij} \in [0, 1]$ for symmetric coupling (for simplicity we assume positive edge weights, but as discussed previously, this is without loss of generality). This, in turn, allows the “regularity” of C to be continuous, $l \in [0, n]$, which allows arbitrary amplification or suppression of the symmetric regularity gap $k_A - k_B$, allowing Δ in the discrete range $\Delta \in \{0, 1/n, 2/n, \dots, 1\}$ and the continuous range $\Delta \in [1, \infty)$. Given Δ^{-1} (discussed in Section 4.2) and arbitrary choice of assignment of a, b , this trivially continuously covers all valid states with $|a^2| + |b|^2 = 1$.

7 Framework Extensions

Beyond real-valued extensions, it is also interesting to study graphs with complex weights, as that is presently the primary distinction between quantum-like and quantum bits. We propose allowing edge weights that are the Gaussian-integer (i.e. complex integer) roots of unity, $e \in \{\pm 1, \pm i\}$. This would allow “regularities” to be complex, affecting what values we are able to represent in Δ , the tuning parameter related to the amplitudes of $|\psi\rangle$. Similar to Section 3.2, this would likely allow amplitude ratios $\Delta \in \mathbb{Q}(i)$, for the Gaussian rationals $\mathbb{Q}(i) = \{a + bi : a, b \in \mathbb{Q}\}$. For the same reason discussed in Section 6, allowing continuous complex edge weights is not interesting.

Additionally, it is interesting to study what single-QL-bit unitary transformations would look like in this framework. We have demonstrated the construction of arbitrary QL-bits directly, but have yet to demonstrate how to get there from an initial state, say $|\psi\rangle = |+\rangle$. Such transformations were implied abstractly in [6] via graph tensor products. It is more interesting to do so while maintaining the same number of nodes and general graph properties (regularity, etc.); explicitly this would be taking our construction of $|\psi\rangle = |+\rangle$ in Lemma 3.1 to $|\psi\rangle = a|+\rangle + b|-\rangle$ in Theorem 3.3.

Finally, it is most natural to extend this work to the two-QL-bit setting.

7.1 Two QL-Bits

Thus far, we have shown explicitly how to construct both a perfect superposition (affirming previous observations) and an arbitrary single-qubit state $|\psi\rangle$. We provide the following intuition for how to extend these efforts to two-qubit states.

As in [32], let G_R be a graph represented by its adjacency matrix R , as illustrated in Figure 7. In this construction, two QL-bits R_0, R_1 are built from four subgraphs $A, B \in R_0, D, E \in R_1$, as expected, with internal bipartite connection matrices $C \in R_0, F \in R_1$. To interact the two QL-bits, we use 4 cross-QL-bit bipartite connection matrices $X_{AD}, X_{AE}, X_{BD}, X_{BE} \in X$ to connect the individual subgraphs of R_0 and R_1 .

This defines the (undirected) block adjacency matrix

$$R = \begin{pmatrix} R_0 & X \\ X^T & R_1 \end{pmatrix}, \quad X := \begin{pmatrix} X_{AD} & X_{AE} \\ X_{BD} & X_{BE} \end{pmatrix}, \quad (46)$$

or, symbolically (and directed),

$$R = \left(\begin{array}{cc|cc} A & A \rightarrow B & A \rightarrow D & A \rightarrow E \\ B \rightarrow A & B & B \rightarrow D & B \rightarrow E \\ \hline D \rightarrow A & D \rightarrow B & D & D \rightarrow E \\ E \rightarrow A & E \rightarrow B & E \rightarrow D & E \end{array} \right), \quad (47)$$

where $A \rightarrow B$ represents edges from A to B .

When R_0, R_1, X are chosen to be regular, we propose that one may use the corresponding quantum-like basis vectors (as defined in Equation (4)) to create the perfect superposition state

$$\psi_{++} \equiv \frac{1}{\sqrt{2}}(|+\rangle + |+\rangle) = \frac{1}{2} \left(\begin{pmatrix} V_A \\ V_B \\ \mathbf{0}_n \\ \mathbf{0}_n \end{pmatrix} + \begin{pmatrix} \mathbf{0}_n \\ \mathbf{0}_n \\ V_D \\ V_E \end{pmatrix} \right) = \frac{1}{2} \begin{pmatrix} V_A \\ V_B \\ V_D \\ V_E \end{pmatrix} \quad (48)$$

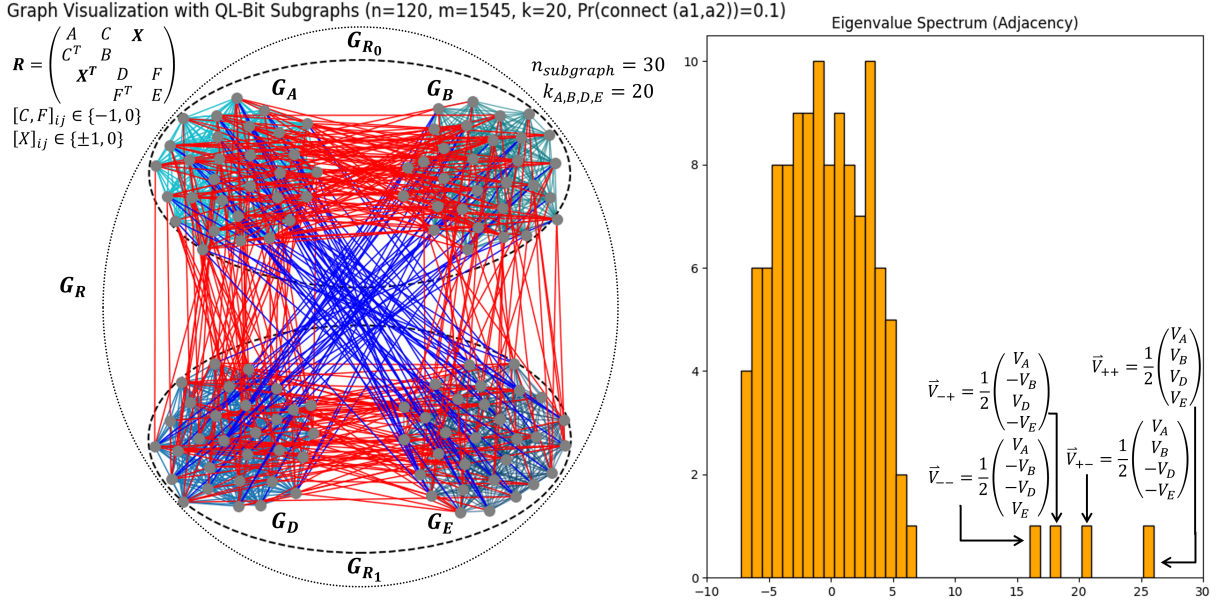


Figure 7: An example of how to connect two QL-bits in the method of [32], along with its adjacency spectrum. See Figure 1 for the single-QL-bit construction. Each subgraph G_A, G_B, G_D, G_E has 30 nodes and is $k = 20$ regular internally. The probability of connection between $G_A \leftrightarrow G_B$ and $G_D \leftrightarrow G_E$ is 0.1 (regularity inside one QL-bit of $20+3$), and between the opposite subgraphs it is 0.05 (average regularity between QL-bits of $1.5+1.5$). Red lines indicate negative edges between $A \leftrightarrow B, A \leftrightarrow D, B \leftrightarrow E, D \leftrightarrow E$, and blue edges indicate positive between the others. See text for more details.

with appropriate eigenvalue $\lambda_{++} = (k+l) + (j_1 + j_2)$ (for k -regular subgraphs R_0 and R_1 , l -regular internal qubit connection graphs C and F , and j -regular qubit-to-qubit connection graph X). This formula is very opaque, but j_1 represents all of the edges going from, for example, $A \rightarrow D$ and j_2 represents $A \rightarrow E$; then the sum $j_1 + j_2$ is the (average block) sum of row 1 of X . Similarly, such a construction would create eigenvectors

$$\psi_{+-} \equiv \frac{1}{\sqrt{2}}(|+\rangle - |-\rangle) = \frac{1}{2} \begin{pmatrix} V_A \\ V_B \\ -V_D \\ -V_E \end{pmatrix}, \quad \psi_{-+} \equiv \frac{1}{\sqrt{2}}(|-\rangle + |+\rangle) = \frac{1}{2} \begin{pmatrix} V_A \\ -V_B \\ V_D \\ -V_E \end{pmatrix}, \quad \psi_{--} \equiv \frac{1}{\sqrt{2}}(|-\rangle - |+\rangle) = \frac{1}{2} \begin{pmatrix} V_A \\ -V_B \\ -V_D \\ V_E \end{pmatrix}, \quad (49)$$

with corresponding eigenvalues $\lambda_{+-} = (k+l) - (j_1 + j_2)$, $\lambda_{-+} = (k-l) + (j_1 - j_2)$, $\lambda_{--} = (k-l) - (j_1 - j_2)$, as illustrated in Figure 7.

We pause to note here that we are (abusively) mapping the algebraic tensor product $|++\rangle$ to the summation of zero-extended basis vectors, as was done in Equation (4). Whether this is the correct extension is open and being studied by the authors, but we know that as the graph expands to N QL-bits, the block adjacency matrix must expand as $2N$. Therefore the eigenvectors, which map to the quantum state, also grow as $2N$.

The goal with two QL-bits is to construct an emergent eigenvector of R corresponding to the arbitrary state

$$|\psi\rangle = a\psi_{++} + b\psi_{+-} + c\psi_{-+} + d\psi_{--} \quad \text{with} \quad |a|^2 + |b|^2 + |c|^2 + |d|^2 = 1.$$

8 Conclusion

We have built upon the framework developed in [31, 32, 35] that defined and showed how to manipulate QL-bits. In particular, we provide mathematically rigorous methods to consistently create arbitrary single QL-states

$$\psi = a\psi_+ + b\psi_-, \quad |a|^2 + |b|^2 = 1$$

without need for ensembles of states. In Section 3, we showed how to create these by manipulating only subgraph regularities, $\Delta = \frac{k_A - k_B}{2l}$. In Section 4, we showed how to do the same by allowing the connecting edges to be directed and manipulating only those regularities, $\Delta_C = \frac{l_A}{l_B}$. In both cases, to prevent unbounded behavior, the introduction of Δ^{-1} and Δ_C^{-1} was necessary along with switching conditions for using each. Finally, in Section 5 we provide an explicit connection between the QL-bit states and random walks on graphs.

Future research opportunities in this area remain broad. In Appendix A, we discuss graph parameters versus spectral gap, and assume spectral gap is known to be constant for distinguishability purposes. While this is sufficient for single QL-bits, many-body systems or systems required to evolve will require more robust spectral guarantees to ensure top eigenvalues remain distinct in the spectrum.

This work is the first to show creation of arbitrary single QL states that scales with the desired precision of the ratio of the amplitudes (as a fraction does to real numbers). Other works have only shown construction of equal superposition in expectation [32] or graph transformations that require taking the Cartesian product of two graphs, an operation which scales exponentially with the number of desired operations and itself requires real edge weights (which this work does not). The authors are currently working on if these techniques can be extended to gates or even single-QL-bit unitaries in a similarly rigorous fashion, as discussed in Section 7.

Given the tight similarities between these QL states and steady states of random walks on a graph, many further directions could be explored from a computer science perspective, in much of the same way as random walks have been explored. While the current construction of different eigenstates does allow us to correlate with the steady state distribution due to the dependence on the diagonal matrix D , an alternate construction that directly manipulates $D^{-1}R$ in order to create state may allow us to better relate the eigenstates to steady states.

Finally, with such a physically fundamental natural concept as spontaneous non-linear synchronization of complex synchronized networks in nature, it could be interesting to see if these networks are performing quantum-like computation at a macro scale. Researchers have long wondered about how quantum processes could drive neurological biological processes [2, 9, 25, 39], this framework could give insights from a more classical perspective.

Acknowledgements

We acknowledge Prof. Gregory D Scholes for insightful discussions. S.K. acknowledges funding from the Office of Science through the Quantum Science Center (QSC), a National Quantum Information Science Research Center.

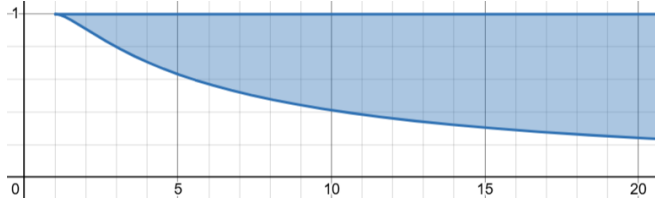


Figure 8: Spectral gap feasible region as a function of graph size n (x-axis) and edge existence probability p (y-axis) for spectral gaps $\lambda_1 - \lambda_2 \geq 1$. Shows minimum graph size as a function of probability of connection; k -regularity is defined as $k = np$, which is λ_1 w.h.p. Reproducible in Appendix B.

Appendices:

A “Large Enough” Spectral Gap

Continuing from the discussion in Section 1, we analyze the spectral gap (Equation (1))

$$\lambda_1 - \lambda_2 \geq np - 2\sqrt{np(1-p)}.$$

The aim of this section is to understand practically when a spectral gap becomes “large enough” to be distinguishable as a parameter of n and p .

Arbitrarily setting a minimum spectral gap

$$|\lambda_1 - \lambda_2| \geq 1,$$

we get the set of constraints

$$1 \leq np - 2\sqrt{np(1-p)}, \quad 0 \leq p \leq 1. \quad (50)$$

Visually, we can see these constraints in Figure 8. Solving Equation (50) for p yields the feasible solution:

$$2\sqrt{\frac{2n-1}{n(n+4)^2}} + \frac{3}{n+4} \leq p \leq 1 \quad \text{for } n \geq 1.$$

Where $n = 1 \implies p = 1$. Equivalently solving for n :

$$n \geq \frac{6 + 2\sqrt{p^2 - 3p + 2}}{p} - 2 \quad \text{for } 0 < p \leq 1. \quad (51)$$

If $p = 0$, there is no graph (the entire matrix is zeros) and therefore no spectral gap. Equation (51) tells us the minimum n given a probability of connection p , as visualized in Figure 8.

Roughly, these equations give the intuition that the regularity k of a graph should not be *too small* compared to the overall graph size n . A big enough k ensures that each QL-bit’s emergent eigenvalues are easily distinguishable (and therefore robust for quantum-like computation).

Precisely, for an arbitrary gap a yielding

$$2\sqrt{\frac{-a^2 + an + n}{n(n+4)^2}} + \frac{a+2}{n+4} \leq p \leq 1 \quad \text{for } n \geq a > 0, \quad (52)$$

we have the following trivial lemma.

Lemma A.1 (Minimum Regularity). *Given a random regular graph of size $n \geq 1$ and edge existence probability p (Erdős-Rényi graph), the minimum average regularity $k = np$ (defined by the minimum p) to achieve a minimum spectral gap of $|\lambda_1 - \lambda_2| \geq a$, for constant a , as $n \rightarrow \infty$ is constant,*

$$\lim_{n \rightarrow \infty} np = 2 + a + 2\sqrt{1+a}. \quad (53)$$

Proof. Follows trivially from limits and Equation (52).

$$\begin{aligned}
\lim_{n \rightarrow \infty} np &\stackrel{(52)}{=} \lim_{n \rightarrow \infty} n \left(2 \sqrt{\frac{-a^2 + an + n}{n(n+4)^2}} + \frac{a+2}{n+4} \right) \\
&= \lim_{n \rightarrow \infty} 2n \sqrt{\frac{-a^2 + an + n}{n(n+4)^2}} + \lim_{n \rightarrow \infty} \frac{an + 2n}{n+4} \\
&= \lim_{n \rightarrow \infty} 2n \sqrt{\frac{-a^2/n + a + 1}{n^2(1 + \frac{4}{n})^2}} + \lim_{n \rightarrow \infty} \frac{a+2}{1 + \frac{4}{n}} \\
&= \left(\lim_{n \rightarrow \infty} 2 \frac{\sqrt{-a^2/n + a + 1}}{1 + \frac{4}{n}} \right) + a + 2 \\
&= 2\sqrt{a+1} + a + 2
\end{aligned}$$

□

This tells us that for any graph size and desired (constant) spectral gap, a random regular graph needs merely constant average regularity of order directly proportional to the gap, $O(a + \sqrt{a}) = O(1)$, to have a spectral gap $\geq a$. For example, if an experimentalist indicates they need a minimum spectral gap of 1 to use these graphs for quantum computation, this says that they need a regularity of $k \geq 6$ no matter the graph size n . For non-constant spectral gaps $A(n)$, loosely speaking, if $A(n)$ converges, the limit converges as above, if $A(n) \in o(n)$ grows slower than n , the limit converges to the limit of $A(n)$ similarly as above, and if $A(n)$ grows similarly or faster than n , the limit either diverges or becomes non-real. In short, the minimum regularity is tightly proportional to the desired spectral gap (as expected). Current simulations of quantum computation using QL-bits only use a constant spectral gap [6].

B Reconstructing Plots with Equations

For Figures 2 and 3:

```

//Made with Desmos 3D (https://www.desmos.com/3d/rh6ae2lkb1)
//Settings --> reverse contrast and translucent surfaces.
x^2+y^2=1 [extend to 3D]
z\ =\ \frac{2xy}{y^2-x^2}\left(\sqrt{x^2+y^2}-1\right)
x\ =\ \sqrt{\frac{1+\sqrt{z^2+1}}{1-\sqrt{z^2+1}}}
x\ =\ -\sqrt{\frac{1+\sqrt{z^2+1}}{1-\sqrt{z^2+1}}}
x\ =\ -\sqrt{\frac{1-\sqrt{z^2+1}}{1+\sqrt{z^2+1}}}
x\ =\ -\sqrt{\frac{1-\sqrt{z^2+1}}{1+\sqrt{z^2+1}}}
z = 1
z = 2
z = -1
z = -2

```

To add visualization of Δ^{-1} beyond Figure 6, as discussed in Section 4.2, add the following equations to the above equations:

```

//(https://www.desmos.com/3d/kzaoepp3j2)
z\ =\ \frac{y^2-x^2}{2xy}\left(\sqrt{x^2+y^2}-1\right)
x\ =\ \sqrt{\frac{1+\sqrt{z^2+1}}{1-\sqrt{z^2+1}}}
x\ =\ -\sqrt{\frac{1-\sqrt{z^2+1}}{1+\sqrt{z^2+1}}}
x\ =\ -\sqrt{\frac{1+\sqrt{z^2+1}}{1-\sqrt{z^2+1}}}
x\ =\ -\sqrt{\frac{1-\sqrt{z^2+1}}{1+\sqrt{z^2+1}}}

```

For Figures 4 and 5

```

//Made with Desmos 3D (https://www.desmos.com/3d/dn7acmpbxr)
//Settings --> reverse contrast and translucent surfaces.
x^2+y^2=1 [extend to 3D]
z\ =\ \frac{x+y}{x-y}\left(\sqrt{x^2+y^2}-1\right) //delta_C
z\ =\ \frac{x-y}{x+y}\left(\sqrt{x^2+y^2}-1\right) //delta_C inverse
x\ =\ \sqrt{z+1}\left(\sqrt{2z^2+2}\right)
x\ =\ -\sqrt{z+1}\left(\sqrt{2z^2+2}\right)

```

```

z = 1
z = 2
z = -1
z = -2

```

For Figure 8:

```

//Made with Desmos (https://www.desmos.com/calculator/ng8ckmfa0b)
2\ \sqrt{\frac{2x-1}{x\left(x+4\right)^2}+\frac{3}{x+4}}\leq y\leq\left(x>1\right)
OR
x\geq2\ \sqrt{\frac{y^2-3y+2}{y^2}}+\frac{3}{y}-2\leq\left(0\leq y\leq1\right)

```

See also: <https://www.wolframalpha.com/input?i=solve+1%3C%3D+xy-2%5Csqrt%7Bxy%281-y%29%7D+for+0%3C%3Dy%3C%3D1> and <https://www.wolframalpha.com/input?i=solve+1%3C%3D+xy-2%5Csqrt%7Bxy%281-y%29%7D%2C+0%3C%3Dy%3C%3D1+for+x>.

C General Characteristic Equation of G_R

This section generalizes the analysis done for Theorem 3.3 and Lemma 4.1.

Lemma C.1. *If we allow G_R to be constructed as before out of two regular subgraphs G_A and G_B , with regularities k_A, k_B , each of order n , with entries $[A]_{ij}, [B]_{ij} \in \{0, 1\}$, coupled by bipartite graph G_C with l_A, l_B -regular directed connection matrices C_A, C_B (with $[C_A]_{ij}, [C_B]_{ij} \in \{-1, 0\}$), then, to ensure*

$$|\psi\rangle := V_R = a|+\rangle + b|-\rangle = \begin{pmatrix} \omega_1 V_A \\ \omega_2 V_B \end{pmatrix}$$

(Equation (10)) is an eigenvector of

$$R = \begin{pmatrix} A & C_A \\ C_B & B \end{pmatrix},$$

$k_A, k_B, l_A, l_B, \omega_1, \omega_2$ must satisfy

$$\omega_2^2 l_A - \omega_1^2 l_B + \omega_1 \omega_2 (k_B - k_A) = 0. \quad (54)$$

by the eigenvector equation. This differs from the lemma and theorem in that all 4 regularities (k_A, k_B, l_A, l_B) are allowed to differ.

Proposition C.2 (Generalization of Symmetric and Asymmetric Coupling for Arbitrary QL-Bits). (a) Theorem 3.3 and (b) Lemma 4.1 are special cases of Equation (54).

Proof. (a) As in Theorem 3.3, take $l_A = l_B$, then Equation (54) becomes

$$(\omega_2^2 - \omega_1^2)l + \omega_1 \omega_2 (k_B - k_A) = 0,$$

yielding

$$\frac{k_A - k_B}{l} = \frac{\omega_2^2 - \omega_1^2}{\omega_1 \omega_2},$$

resulting in Equations (9) and (11).

(b) As in Lemma 4.1, take $k_A = k_B$, then Equation (54) becomes

$$\omega_2^2 l_A - \omega_1^2 l_B = 0,$$

yielding

$$\frac{\omega_1^2}{\omega_2^2} = \frac{l_A}{l_B},$$

resulting in Equations (26) and (27). □

This shows that an arbitrary QL-bit can be constructed by two regular subgraphs joined by two regular directed bipartite connection matrices, as long as the regularities k_A, k_B, l_A, l_B are related to the quantum state amplitudes ω_1, ω_2 by Equation (54).

References

- [1] Suman Acharyya, Priodyuti Pradhan, and Chandrakala Meena. 2025. Master Stability Functions in Complex Networks. arXiv:2412.19163 [nlin.AO] <https://arxiv.org/abs/2412.19163>
- [2] Betony Adams and Francesco Petruccione. 2020. Quantum effects in the brain: A review. *AVS Quantum Science* 2, 2 (04 2020), 022901. <https://doi.org/10.1116/1.5135170> arXiv:https://pubs.aip.org/avs/aqs/article-pdf/doi/10.1116/1.5135170/13961165/022901_1.online.pdf
- [3] Noga Alon. 1986. Eigenvalues and expanders. *Combinatorica* 6, 2 (1986), 83–96.
- [4] Johannes Alt, Raphaël Ducatez, and Antti Knowles. 2021. Extremal eigenvalues of critical Erdős–Rényi graphs. *The Annals of Probability* 49, 3 (2021), 1347 – 1401. <https://doi.org/10.1214/20-AOP1483>
- [5] Graziano Amati and Gregory D. Scholes. 2025. Encoding quantum-like information in classical synchronizing dynamics. arXiv:2504.03852 [quant-ph] <https://arxiv.org/abs/2504.03852>
- [6] Graziano Amati and Gregory D. Scholes. 2025. Quantum information with quantumlike bits. *Phys. Rev. A* 111 (Jun 2025), 062203. Issue 6. <https://doi.org/10.1103/PhysRevA.111.062203> <https://arxiv.org/abs/2408.06485>.
- [7] Alex Arenas, Albert Díaz-Guilera, Jurgen Kurths, Yamir Moreno, and Changsong Zhou. 2008. Synchronization in complex networks. *Physics reports* 469, 3 (2008), 93–153.
- [8] Mauricio Barahona and Louis M Pecora. 2002. Synchronization in small-world systems. *Physical review letters* 89, 5 (2002), 054101.
- [9] Friedrich Beck and John C Eccles. 1998. Quantum processes in the brain: A scientific basis of consciousness. *Cognitive Studies: Bulletin of the Japanese Cognitive Science Society* 5, 2 (1998), 2_95–2_109.
- [10] Francesco Belardo, Sebastian M. Cioabă, Jack Koolen, and Jianfeng Wang. 2018. Open problems in the spectral theory of signed graphs. *The Art of Discrete and Applied Mathematics* 1, 2 (2018), #P2.10. <https://doi.org/10.26493/2590-9770.1286.d7b>
- [11] Rajendra Bhatia. 1997. Matrix Analysis. *Graduate Texts in Mathematics* 169 (1997), 360. <https://link.springer.com/book/10.1007/978-1-4612-0653-8>.
- [12] Stefano Boccaletti. 2008. The Synchronized Dynamics of Complex Systems. In *The Synchronized Dynamics of Complex Systems*, Stefano Boccaletti (Ed.). Monograph Series on Nonlinear Science and Complexity, Vol. 6. Elsevier, Amsterdam, Netherlands, 1–239. [https://doi.org/10.1016/S1574-6917\(07\)06001-1](https://doi.org/10.1016/S1574-6917(07)06001-1)
- [13] Béla Bollobás. 1998. *Random Graphs*. Springer New York, New York, NY, 215–252. https://doi.org/10.1007/978-1-4612-0619-4_7
- [14] Fan Chung, Linyuan Lu, and Van Vu. 2003. Spectra of random graphs with given expected degrees. *Proceedings of the National Academy of Sciences* 100, 11 (2003), 6313–6318.
- [15] Gábor Csárdi, Tamás Nepusz, Vincent Traag, Szabolcs Horvát, Fabio Zanini, Daniel Noom, and Kirill Müller. 2025. *igraph: Network Analysis and Visualization in R*. Comprehensive R Archive Network. <https://doi.org/10.5281/zenodo.7682609> R package version 2.1.4; sample_gnp() reference at https://r.igraph.org/reference/sample_gnp.html.
- [16] Paul L. Erdos and Alfréd Rényi. 1959. On random graphs I. *Publicationes Mathematicae Debrecen* 6 (1959), 290–297. https://static.renyi.hu/~p_erdos/1959-11.pdf
- [17] László Erdős, Antti Knowles, Horng-Tzer Yau, and Jun Yin. 2013. Spectral statistics of Erdős–Rényi graphs I: Local semicircle law. *The Annals of Probability* 41, 3B (2013), 2279 – 2375. <https://doi.org/10.1214/11-AOP734>
- [18] Victor Hugo F. Francheto. 2024. Synchronization in complex networks. <https://medium.com/@victor.h.f.francheto/synchronization-in-complex-networks-17e4380432ce>
- [19] Joel Friedman. 2003. Relative expanders or weakly relatively Ramanujan graphs. *Duke Mathematical Journal* 118, 1 (2003), 19–35.
- [20] Zoltán Füredi and János Komlós. 1981. The eigenvalues of random symmetric matrices. *Combinatorica* 1 (1981), 233–241.

[21] Lucia Valentina Gambuzza, Francesca Di Patti, Luca Gallo, Stefano Lepri, Miguel Romance, Regino Criado, Mattia Frasca, Vito Latora, and Stefano Boccaletti. 2021. Stability of synchronization in simplicial complexes. *Nature communications* 12, 1 (2021), 1255.

[22] Chris Godsil and Gordon F Royle. 2013. *Algebraic graph theory*. Vol. 207. Springer Science & Business Media, New York, Chapter 9, 193–216.

[23] Alice Guionnet. 2021. Bernoulli Random Matrices. In *European Congress of Mathematics 2021*. EMS Press, Room MA266, Institut für Mathematik, Technische Universität Berlin, Straße des 17. Juni 136, 10623 Berlin, Germany, 45–71.

[24] Jiaoyang Huang, Theo McKenzie, and Horng-Tzer Yau. 2024. Optimal Eigenvalue Rigidity of Random Regular Graphs. arXiv:2405.12161 [math.PR] <https://arxiv.org/abs/2405.12161>

[25] Peter Jedlicka. 2017. Revisiting the quantum brain hypothesis: toward quantum (neuro) biology? *Frontiers in molecular neuroscience* 10 (2017), 366.

[26] Ferenc Juhász. 1978. On the spectrum of a random graph. In *Algebraic Methods in Graph Theory*. Colloquia Mathematica Societatis János Bolyai, Vol. 25. North-Holland Publishing Co. and János Bolyai Mathematical Society, Amsterdam and Budapest, 313–316. <https://real.mtak.hu/35450/>

[27] László Lovász. 1993. Random walks on graphs. *Combinatorics, Paul Erdős is eighty* 2, 1-46 (1993), 4.

[28] A. Nilli. 1991. On the second eigenvalue of a graph. *Discrete Mathematics* 91, 2 (1991), 207–210. [https://doi.org/10.1016/0012-365X\(91\)90112-F](https://doi.org/10.1016/0012-365X(91)90112-F)

[29] Louis M Pecora and Thomas L Carroll. 1998. Master stability functions for synchronized coupled systems. *Physical review letters* 80, 10 (1998), 2109.

[30] S Unnikrishna Pillai, Torsten Suel, and Seunghun Cha. 2005. The Perron-Frobenius theorem: some of its applications. *IEEE Signal Processing Magazine* 22, 2 (2005), 62–75.

[31] Gregory D. Scholes. 2023. Large Coherent States Formed from Disordered k-Regular Random Graphs. *Entropy* 25, 11 (2023), 1519. <https://doi.org/10.3390/e25111519>

[32] Gregory D Scholes. 2024. Quantum-like states on complex synchronized networks. *Proceedings of the Royal Society A* 480, 2295 (2024), 20240209.

[33] Gregory D. Scholes. 2025. Dynamics in an emergent quantum-like state space generated by a nonlinear classical network. arXiv:2501.07500 [quant-ph] <https://arxiv.org/abs/2501.07500>

[34] Gregory D Scholes. 2025. Graphs that predict exciton delocalization. arXiv:2501.09843 [chem-ph] <https://arxiv.org/abs/2501.09843>

[35] Gregory D. Scholes and Graziano Amati. 2025. Quantumlike Product States Constructed from Classical Networks. *Phys. Rev. Lett.* 134 (Feb 2025), 060202. Issue 6. <https://doi.org/10.1103/PhysRevLett.134.060202>

[36] Shir Shahal, Ateret Wurzberg, Inbar Sibony, Hamootal Duadi, Elad Shniderman, Daniel Weymouth, Nir Davidson, and Moti Fridman. 2020. Synchronization of complex human networks. *Nature Communications* 11, 1 (2020), 3854. <https://doi.org/10.1038/s41467-020-17540-7>

[37] Steven H Strogatz. 2000. From Kuramoto to Crawford: exploring the onset of synchronization in populations of coupled oscillators. *Physica D: Nonlinear Phenomena* 143, 1-4 (2000), 1–20.

[38] Yang Tang, Feng Qian, Huijun Gao, and Jürgen Kurths. 2014. Synchronization in complex networks and its application – A survey of recent advances and challenges. *Annual Reviews in Control* 38, 2 (2014), 184–198. <https://doi.org/10.1016/j.arcontrol.2014.09.003>

[39] Max Tegmark. 2000. Importance of quantum decoherence in brain processes. *Physical review E* 61, 4 (2000), 4194.

[40] V. H. Vu. 2005. Spectral norm of random matrices. In *Proceedings of the Thirty-Seventh Annual ACM Symposium on Theory of Computing* (Baltimore, MD, USA) (STOC '05). Association for Computing Machinery, New York, NY, USA, 423–430. <https://doi.org/10.1145/1060590.1060654>